2021 43rd Annual International Conference of the
IEEE Engineering in Medicine & Biology Society (EMBC)
Oct 31 - Nov 4, 2021. Virtual Conference

Numerical estimation of the B1 transmit field distortion in a copper EEG trace comparison with the thin-film based resistive trace "NeoNet"

Hongbae Jeong, and Giorgio Bonmassar, *Senior Member, IEEE*

***Abstract*— This study investigates the effects of EEG traces in B1 transmit field distortion in a 3T MRI. EEG is a non-invasive method to monitor brain activities. Although EEG monitors brain activities with a high temporal resolution, it has trouble localizing the signal source. The EEG-fMRI is the multimodal imaging method, but care is needed to use EEG while in MRI as EEG traces create the signal distortion to the MRI. To tackle this problem, resistive traces are developed using thin-film technology to reduce the signal distortion during MRI. Numerical simulation was used to estimate the amount of B1 transmit field distortion of NeoNet and copper-based EEG nets (CuNet - with and without current limiting resistors) compared with the case without EEG net (NoNet). The reduced B1 transmit field distortion is estimated in the case of NeoNet compared to the CuNets. NeoNet is an MR-compatible high-density EEG net designed for pediatric subjects. The proposed NeoNet traces will facilitate/enable such EEG/fMRI pediatric studies with mitigated artifacts, which in turn will help to move the pediatric EEG/fMRI field forward.**

***Clinical Relevance*—This study estimates the benefit of the thin-film based EEG net with reduced B1 transmit artifact for the multimodal study of EEG-fMRI. The results are compared with commercial EEG trace made with copper metal with current limiting resistors. It is reported that about 470,000 children are suffering from Epilepsy. The MR-compatible resistive EEG traces se EEG-fMRI has potential to be a valuable tool to help understand pediatric Epilepsy and move the pediatric EEG-fMRI field forward**

I. Introduction

It is reported that about 470,000 children are affected by Epilepsy [1]. For these pediatric patients, continuous video EEG provides particularly useful information on the neurological status and can identify electroencephalographic seizures. Despite that EEG provides functional and diagnostic information, it often needs to be complemented with neuroimaging techniques such as MRI that can deliver complete anatomic coverage of the brain [2]. MRI is used to provide supplementary information by demonstrating contrast enhancement in inflammatory areas or assessing tissue viability and metabolic processes by the use of diffusion-weighted imaging (DWI) and MR spectroscopy. However, currently, EEG electrode caps/nets are required to be removed before neuroimaging since EEG produces visible and significant artifacts that can compromise the quality of MRI.

Thin-film is an exciting method to fabricate nano-scale electric traces and circuits. The EEG trace using thin-film could be used to make EEG traces invisible in MRI while EEG signal can be obtained. In this study we conducted series of numerical simulations to estimate the effects of thin-film based EEG trace on a 29-month-old child using a finite-difference time-domain (FDTD) method. The results of thin-film based EEG trace (NeoNet) is compared with NoNet, CuNet (without resistors), and CuNet (with ideal current limiting resistors). The B1 transmit field distortion of an image-compatible and state-of-the-art high-density thin-film based pediatric EEG net, the "NeoNet".

II. Materials and Method

A. EEG trace design

The resistive EEG trace was fabricated using the thin-film aluminum (thickness: 30nm) coated on a polyamide with a target resistance of 11 kΩ (**Fig. 1**). The dielectric properties of the resistive EEG traces (NeoNet) were chosen as $\sigma = 46.30$ S/m, and relative permittivity (ε_r) of 4.2, while $\sigma = 5.7 \cdot 10^7$ S/m and relative permittivity of $\varepsilon_r = 4.2$ for the copper EEG net (CuNet). The properties of electrodes (i.e., sponges) soaked in KCl solution were chosen for $\sigma = 2.14$ S/m, $\varepsilon_r = 84.7$, respectively [3]. Total of 128-channel traces were designed to use in pediatric EEG-fMRI studies.

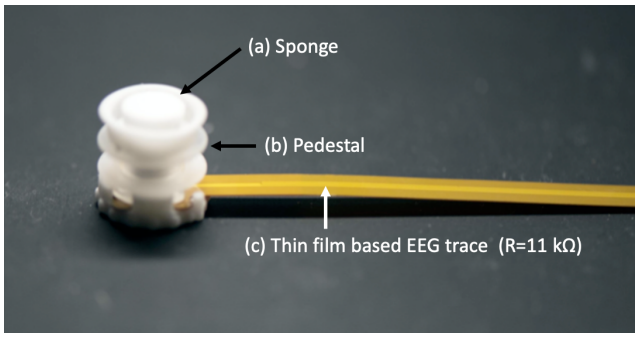

Figure 1: Fabricated EEG trace. (a) Sponge bridging the contact between skin and the electrode, (b) Pedestal to hold the structure of the sponge, (c) Thin-film based EEG trace (R=11 kΩ)

B. Numerical simulation

The Sim4Life (ZMT MedTech, Switzerland) was used to solve Maxwell's equation at 128 MHz using a FDTD method [4]. The birdcage body transmit coil with a shield (Coil

*Research supported by NIH/NIBIB grant R01EB024343.

H. Jeong is with A. Martinos Center for Biomedical Imaging, Charlestown, MA 02129 USA (e-mail: hjeong3@ mgh.harvard.edu).

G. Bonmassar is with the A. Martinos Center for Biomedical Imaging, Massachusetts General Hospital/Harvard Medical School, Charlestown, MA 02129 USA (corresponding author to provide phone: 617-726-0962; fax: 617-726-7462; e-mail: Giorgio.bonmassar@mgh.harvard.edu).

diameter: 610mm , length: 670 mm, shield diameter: 660 mm, length : 1220 mm) was designed with a realistic dimension using in 3 T MRI [5]. The input current was driven in the circularly polarized (CP) mode. The head of the 29-month-old male whole-body voxel model was positioned at the center of the body coil to assess the complex B1 field behaviors in the pediatric tissues [6].

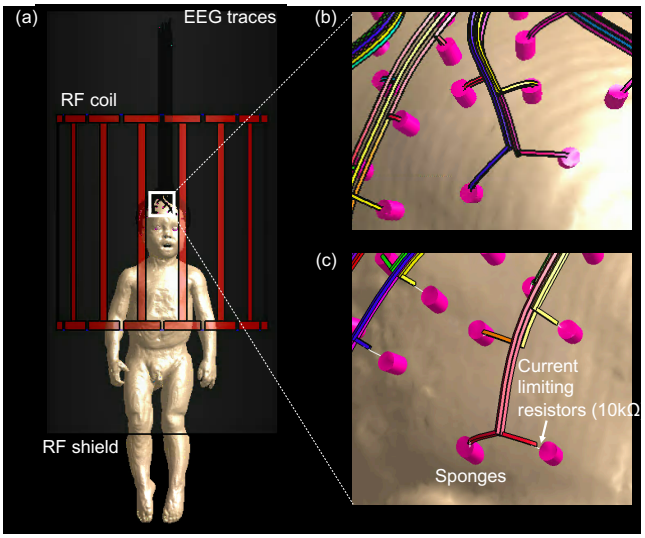

Figure 2: Coil and EEG geometry. (a) shows the simulation view of the 29-month-old male model positioned at the center of the body transmit coil, (b) shows the drawing of the EEG traces without current limiting resistors, (c) shows the EEG traces with current limiting resistors.

128-channel EEG traces were drawn on the head of the pediatric model following from the temporal lobe towards the parietal lobe, traveling through the top of the head (**Fig. 2**). The trace width was chosen to represent 11 kΩ as the actual trace thickness is not achievable to draw (i.e., 30 nm), and each trace was designed to have a minimum distance of 1 mm from each other and also from the skin to avoid in contact between traces and the skin (**Fig. 2**b). The locally dense grid was applied along the traces with the grid resolution of 0.7 mm × 0.7 mm ×1.0 mm. The high-performance GPU (NVIDIA V10, MA) was used to accelerate the computation time. The B1 transmit fields were computed in four different scenarios: (i) a pediatric model without an EEG net (NoNet), (ii) with a thin-film based EEG net (NeoNet), (iii) with copper traces with an ideal current limiting resistor (R=10kΩ) between sponges and copper traces (CuNet), (iv) with a copper traces without current limiting resistors. The B1 transmit field and current density was normalized to field that produced 2μT at the center of the coil in case of NoNet. Same input currents are applied to the all other cases. B1 transmit filed ,and current density map are compared to estimate the effect of the difference EEG traces.

III. RESULTS

The axial, coronal, and sagittal view of the absolute B1 transmit field was compared in **Fig**. 3. The B1 transmit field distribution on the child model and the air was shown without a mask. **Fig. 4** shows the difference in absolute B1 transmit fields between (i) NoNet vs. NeoNet, (ii) NoNet vs. CuNet with ideal current limiting resistances, and (iii) NoNet vs. CuNet without resistors are compared in axial, coronal, and sagittal view. Masks were applied on the surrounding air which allows ones to see the B1 transmit field difference in the child model.

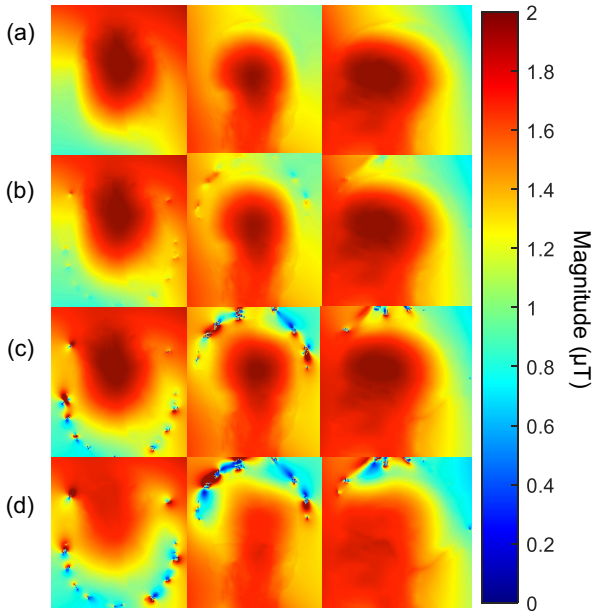

Figure 3. Simulated B1 transmit field distribution from the pediatric model in Axial (left), Coronal (middle), and Sagittal (right) view in case of (a) NoNet, (b) NeoNet, (c) CuNet with ideal current limiting resistors. (d) CuNet without resistors.

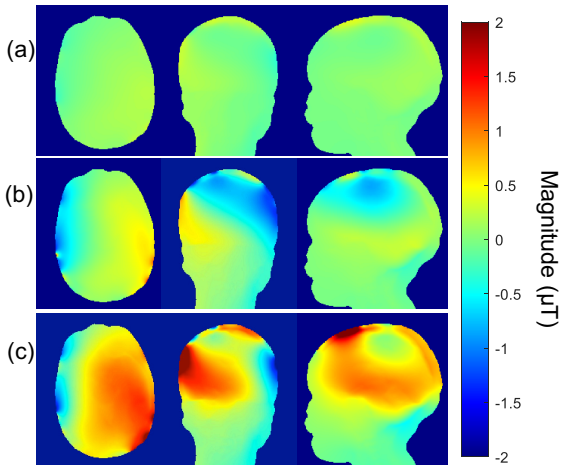

Figure 4: Difference in absolute B1 transmit field distribution in Axial, Coronal, and sagittal view in case of (a) NoNet - NeoNet, (b) NoNet – CuNet with ideal current limiting resistors, and (c) NoNet – CuNet without resistors

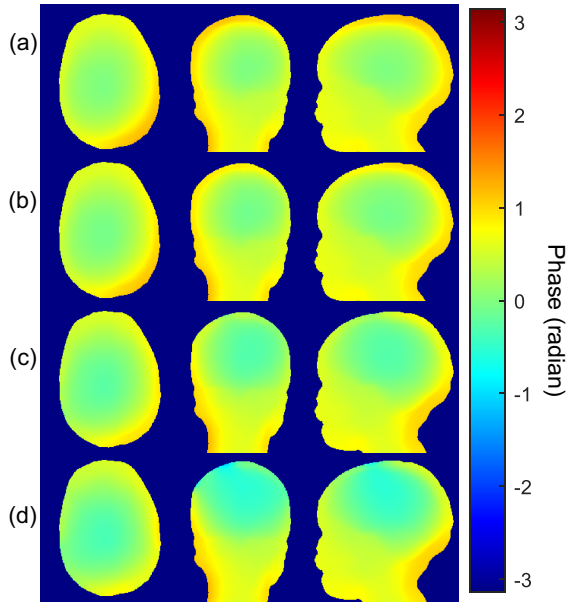

Figure 5: Phase map of the B1 transmit field in case of (a) NoNet, (b) NeoNet, (c) CuNet with ideal current limiting resistors, and (d) CuNet without resistors

Fig. 5 shows the phase of the B1 transmit field in aixial, coronal, and sagittal view in case of NoNet, NeoNet, CuNet with ideal current limiting resistors, and CuNet without resistors. The difference in phase of the B1 transmit field between (i) NoNet vs. NeoNet, (ii) NoNet vs. CuNet with ideal current limiting resistors, and (iii) NoNet vs. CuNet without resistors are also compared in **Fig** 6.

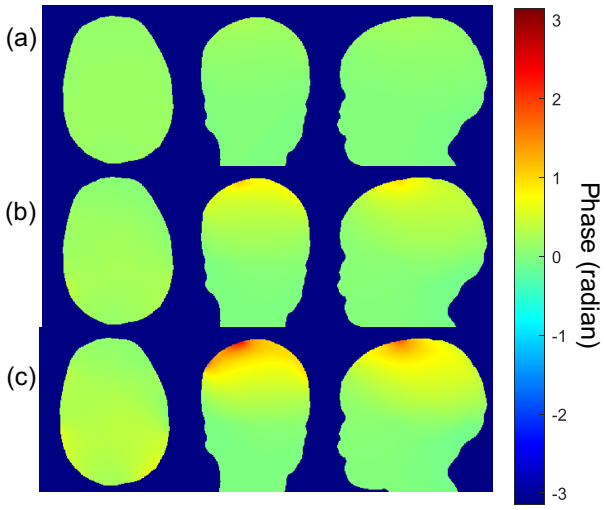

Figure 6: Difference in a phase of the B1 transmit field in case of (a) NoNet - NeoNet, (b) NoNet – CuNet with ideal current limiting resistors, and (c) NoNet – CuNet without resistors

Fig. 7 shows the B1 transmit field profile in NoNet, NeoNet, CuNet with and without current limiting resistors.

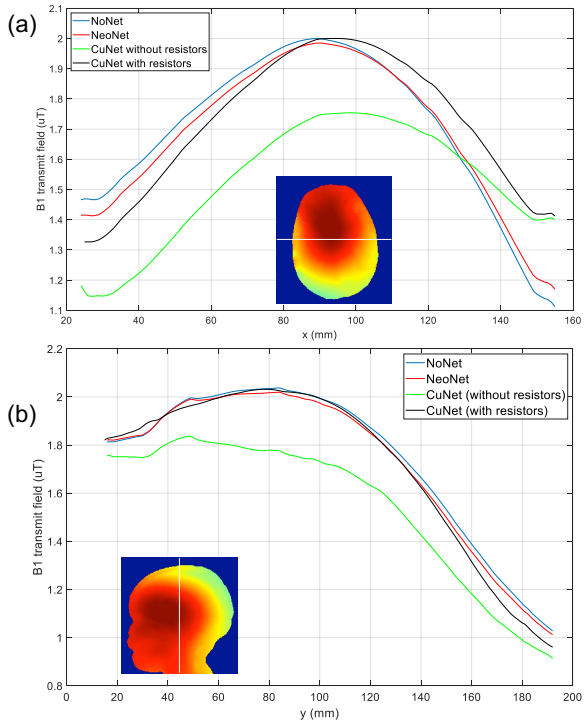

Figure 7: Comparison of the B1 transmit field among four cases in (a) axial profile, and (b) longitudinal profile.

The current density map is displayed along the three EEG trace scenarios with 3D surface view in **Fig.** 8

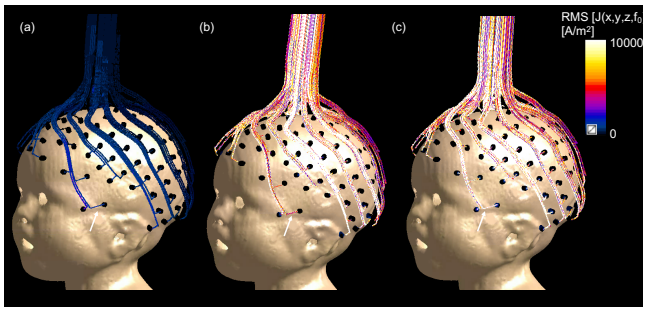

Figure 8: Current density map displayed on EEG traces in 3D surface view. (a) NeoNet, (b) CuNet with ideal current limiting resistors, (c) CuNet without resistors.

The averaged and covariance of B1 field uniformity in the head was compared in **Table** 1. The standard deviation was divided by the averaged B1 transmit field in the head to compute the B1 transmit field covariance.

TABLE I. INTENSITY ANALYSIS OF THE B1 TRANSMIT FIELD

	B1 transmit field uniformity			
	NoNet	***NeoNet Introduction***	***CuNet (with ideal resistors)***	***CuNet (without resistors)***
Mean B_1^+ field (μT)	0.1537	0.1533	0.1567	0.1460
B_1^+ covariance (A.U.)*	5.8261	5.7071	6.1165	5.0763

*A.U. stands for arbitrary unit (no unit)

Uncertainties analysis is conducted to see the sensitivity of the simulation parameter (Table II).

TABLE II. UNCERTAINTY ANALYSIS

Mean B_1^+	**Uncertainty of the mean B1 transmit field estimation**						
	Val1	***Val2***	***Result 1 (μT)***	***Result 2 (μT)***	***Sensitivity Factor***	***Std. Dev.***	***Uncertainty (%)***
Muscle cond. [S/m]	0.96	0.87	1.533	1.533	0.04	0.00	0.00
Muscle perm.	85.24	76.72	1.533	1.530	2.8	0.021	0.069
Skin cond. [S/m]	0.65	0.59	1.533	1.535	0.04	0.007	0.041
Skin perm.	118.90	107.00	1.533	1.529	2.8	0.027	0.065
SAT cond. [S/m]	0.10	0.09	1.533	1.534	0.04	0.007	0.267
SAT perm.	15.09	13.58	1.533	1.529	2.8	0.025	0.460

The methods used were based on the work of Neufeld et al. [7] *to evaluate the uncertainty of the quantities derived by simulation, two simulations were assessed for each parameter by assigning two different values ("Value 1" and "Value 2"). The first value ("Value1") was the one used for the simulation shown in* ***Table I****, whereas the second value ("Value2") was set to a realistic value that could occur from measurement or design choice. The results obtained for each value ("Result1", and "Result 2") were used to evaluate the sensitivity factor of the quantity evaluated (mean B1transmit field). The standard deviation ("Std. Dev.") was derived from literature.*

IV. DISCUSSION AND CONCLUSION

The study reports the numerical estimation of the B1 transmit field distortion on a 29-month-old male model wearing 128-channel hd-EEG nets in a 3 Tesla MRI. The series of electromagnetic (EM) simulations were conducted on a child model to estimate the B1 transmit field distortion in the case of resistive EEG trace (NeoNet), CuNet with ideal current limiting resistors, and CuNet without current limiting resistors. The results shows that NeoNet has the marginal difference of the B1 transmit field distortion compared to the case of NoNet, whereas the CuNet is estimated producing noticeable B1 transmit field distortion at 3T MRI. Additionally, current density maps on three different EEG traces scenarios were compared to estimate the amount of current attracted on each EEG traces. CuNet without resistor attracted the biggest amount of current among three, whereas the CuNet with ideal current limiting resistors were estimated to mitigate the current at the end of the trace. The NeoNet was estimated to produce the lowest current compared to the case of CuNet. In the case of CuNet without current limiting resistors, overall B1 transmit field on pediatric head tends reduced due to the shielding effect. Whereas the case of CuNet with ideal current limiting resistors EEG traces are acting as an "antenna" while estimated showing the reduced current density at the end of the EEG trace compared to the CuNet without current limiting resistors. Although, resistive trace was estimated to produce the most similar B1 transmit field interaction to the case of NoNet, which could be explained by significantly reduced current density estimated on the resistive trace compared to the cases of CuNet.

Limitation: This study contains following limitations. Resistors behaves as series inductors and parallel capacitors on top of the self-resistance at high frequency which is not accounted at this numerical simulation. Thus, the B1 transmit field in the case of CuNet without current limiting resistors showed the more similar to the real case [8], [9]. The EEG traces were treated as open-ended circuit which might be different when EEG is connected to the amplifiers during MRI experiment. The effect of the EEG traces with different trajectories are not considered at the study. Finally, the experimental validation need to be completed to confirm the findings in this study.

V. CONCLUSION

The reduced B1 transmit field distortion is estimated in the case of NeoNet compared to the CuNet. NeoNet is an MR-compatible high-density EEG net designed for pediatric subjects. The proposed NeoNet traces has potential to facilitate/enable EEG/fMRI pediatric studies with mitigated artifacts, which in turn will help to move the pediatric EEG/fMRI field forward.

ACKNOWLEDGMENT

This work was supported by the NIH/ NIBIB grant R01EB024343. Authors acknowledge to "Sim4Life by ZMT, www.zurichmeditech.com" for Science License.

REFERENCES

[1] M. M. Zack and R. Kobau, "National and State Estimates of the Numbers of Adults and Children with Active Epilepsy — United States, 2015," *MMWR. Morb. Mortal. Wkly. Rep.*, vol. 66, no. 31, pp. 821–825, Aug. 2017.

[2] N. E. Fultz *et al.*, "Coupled electrophysiological, hemodynamic, and cerebrospinal fluid oscillations in human sleep," *Science (80-.).*, vol. 366, no. 6465, pp. 628–631, 2019.

[3] S. R. Atefi, P. Serano, C. Poulsen, L. M. Angelone, and G. Bonmassar, "Numerical and Experimental Analysis of Radiofrequency-Induced Heating Versus Lead Conductivity During EEG-MRI at 3 T," *IEEE Trans. Electromagn. Compat.*, vol. 61, no. 3, pp. 852–859, 2019.

[4] K. S. Yee, "Numerical Solution of Initial Boundary Value Problems Involving Maxwell's Equations in Isotropic Media," *IEEE Trans. Antennas Propag.*, vol. 14, no. 3, pp. 302–307, 1966.

[5] P. Serano, L. M. Angelone, H. Katnani, E. Eskandar, and G. Bonmassar, “A novel brain stimulation technology provides compatibility with MRI,” *Sci. Rep.*, vol. 5, no. 1, p. 9805, Sep. 2015.

[6] H. Jeong *et al.*, “Development, validation, and pilot MRI safety study of a high-resolution, open source, whole body pediatric numerical simulation model,” *PLoS One*, vol. 16, no. 1, p. e0241682, Jan. 2021.

[7] E. Neufeld, S. Kühn, G. Szekely, and N. Kuster, “Measurement, simulation and uncertainty assessment of implant heating during MRI,” *Phys. Med. Biol.*, vol. 54, no. 13, pp. 4151–4169, Jul. 2009.

[8] C. Poulsen, D. G. Wakeman, S. R. Atefi, P. Luu, A. Konyn, and G. Bonmassar, “Polymer thick film technology for improved simultaneous dEEG/MRI recording: Safety and MRI data quality: Polymer Thick Film Technology for Improved dEEG/MRI,” *Magn. Reson. Med.*, vol. 77, no. 2, pp. 895–903, 2017.

[9] N. E. Fultz *et al.*, “High-quality FLAIR and diffusion imaging with presence of EEG nets,” in *International Society for Magnetic Resonance in Medicine*, 2019, p. 3116.